

Assay Services **All Things Interferon** Knowledge
Kits & Reagents
pbl Interferon source
20 Years of Interferon Excellence 1.877.725.8881 www.interferonsource.com



Characterizing the Dynamics of CD4+ T Cell Priming within a Lymph Node

Jennifer J. Linderman, Thomas Riggs, Manjusha Pande, Mark Miller, Simeone Marino and Denise E. Kirschner

This information is current as of December 2, 2010

J Immunol 2010;184:2873-2885; Prepublished online 12 February 2010;

doi:10.4049/jimmunol.0903117

<http://www.jimmunol.org/content/184/6/2873>

-
- References** This article cites **76 articles**, 30 of which can be accessed free at: <http://www.jimmunol.org/content/184/6/2873.full.html#ref-list-1>
- Subscriptions** Information about subscribing to *The Journal of Immunology* is online at <http://www.jimmunol.org/subscriptions>
- Permissions** Submit copyright permission requests at <http://www.aai.org/ji/copyright.html>
- Email Alerts** Receive free email-alerts when new articles cite this article. Sign up at <http://www.jimmunol.org/etoc/subscriptions.shtml/>



Characterizing the Dynamics of CD4+ T Cell Priming within a Lymph Node

Jennifer J. Linderman,^{*,†,‡} Thomas Riggs,[§] Manjusha Pande,[§] Mark Miller,[¶] Simeone Marino,[§] and Denise E. Kirschner^{‡,§}

Generating adaptive immunity postinfection or immunization requires physical interaction within a lymph node T zone between Ag-bearing dendritic cells (DCs) and rare cognate T cells. Many fundamental questions remain regarding the dynamics of DC–CD4+ T cell interactions leading to priming. For example, it is not known how the production of primed CD4+ T cells relates to the numbers of cognate T cells, Ag-bearing DCs, or peptide-MHCII level on the DC. To address these questions, we developed an agent-based model of a lymph node to examine the relationships among cognate T cell frequency, DC density, parameters characterizing DC–T cell interactions, and the output of primed T cells. We found that the output of primed CD4+ T cells is linearly related to cognate frequency, but nonlinearly related to the number of Ag-bearing DCs present during infection. This addresses the applicability of two-photon microscopy studies to understanding actual infection dynamics, because these types of experiments increase the cognate frequency by orders of magnitude compared with physiologic levels. We found a trade-off between the quantity of peptide-major histocompatibility class II on the surface of individual DCs and number of Ag-bearing DCs present in the lymph node in contributing to the production of primed CD4+ T cells. Interestingly, peptide-major histocompatibility class II $t_{1/2}$ plays a minor, although still significant, role in determining CD4+ T cell priming, unlike the primary role that has been suggested for CD8+ T cell priming. Finally, we identify several pathogen-targeted mechanisms that, if altered in their efficiency, can significantly effect the generation of primed CD4+ T cells. *The Journal of Immunology*, 2010, 184: 2873–2885.

The adaptive immune response to pathogen infection is dependent on generation of primed CD4+ T cells in the lymph node (LN). Dendritic cells (DCs) in tissues take up pathogens and present antigenic peptides on their surface in the context of major histocompatibility class II molecules (peptide-MHCII complexes [pMHCII]) (1–3). These Ag-bearing DCs migrate via afferent lymphatics to the closest tissue-draining LN. T cells constantly transit between the circulatory and lymphatic systems, entering individual LNs via high endothelial venules and re-entering the circulatory system via the thoracic duct from efferent lymphatics (4). Generation of primed CD4+ T cells requires contact between these Ag-bearing DCs and specific (cognate) CD4+ T cells; their successful binding leads to CD4+ T cell priming (5). Whereas DCs rarely leave the LN, primed CD4+ T cells exit the LN and return to the site of infection to participate in the immune response.

Despite a wealth of information on the immune response, including studies on the dynamics of DC–T cell interactions in a LN via two-photon microscopy (2PM) (3, 6, 7), many fundamental questions remain regarding the functioning of the LN. For example, it is not known how the production of primed CD4+ T cells is related to the numbers of cognate CD4+ T cells, Ag-bearing DCs, or pMHCII level on the DC surface. Will doubling the number of cognate CD4+ T cells or Ag-bearing DCs double the primed CD4+ T cell output? Experimental preparations such as 2PM often increase the density of cognate CD4+ T cells or DCs beyond the physiologic range to facilitate observation (8, 9), so answering this question will indicate how information from these studies can be interpreted. Do high numbers of DCs with fewer pMHCII give equivalent CD4+ T cell priming as low numbers of DCs with more pMHCII? Answering this question would give insight into the relationship between Ag dose and T cell priming. A few recent studies have explored these questions for CD8+ T cells (10, 11). However, CD8+ T cells recognize Ag presented on DCs in the context of peptide-MHC class I (pMHCI) molecules. The $t_{1/2}$ of pMHCI is on the order of a few hours; it is not surprising then that pMHCI $t_{1/2}$ profoundly affects the extent and dynamics of CD8+ T cell priming (10, 11). Interestingly, the $t_{1/2}$ of pMHCII is on the order of days (12–14)—that is, it is extended beyond the lifespan of the DC in most cases. Therefore, additional processes and parameters might play important and undiscovered roles in driving CD4+ T cell priming dynamics. Several recent computational studies have focused on the details of cell movement within a lymphoid organ (10, 15–17). In contrast, our study focuses on functionality of the LN during exposure to Ag.

Pathogenic microbes can interfere with the immune response via several mechanisms related to DC–T cell interactions (e.g., reduction of pMHCII on the DC surface during infection with *Mycobacterium tuberculosis* or interference with trafficking of DCs to the LN) (18, 19). Therefore, understanding the relationships between the quantities outlined above—numbers of CD4+ T cell and

*Department of Chemical Engineering, [†]Department of Biomedical Engineering, [‡]Center for Computational Medicine and Bioinformatics, and [§]Department of Microbiology and Immunology, University of Michigan, Ann Arbor, MI 48109; and [¶]Department of Pathology and Immunology, Washington University School of Medicine, St. Louis, MO 63130

Received for publication September 23, 2009. Accepted for publication December 17, 2009.

This work was supported by National Institutes of Health Grants HL68526, HL72682, NO1 A150018, LM00902701, HL092853, and HL092844.

Address correspondence and reprint requests to Denise E. Kirschner, University of Michigan Medical School, 6730 Medical Science Building II, 1150 W. Medical Center Drive, Ann Arbor, MI 48109-5620. E-mail address kirschne@umich.edu

Abbreviations used in this paper: 2D, two-dimensional; 2PM, two-photon microscopy; Ab-DC, antigen-bearing dendritic cell; ABM, agent-based model; Cog, cognate frequency; DC, dendritic cell; HEV, high endothelial venule; IDC, immature dendritic cell; LDC, licensed dendritic cell; LHS, Latin hypercube sampling; LN, lymph node; MS, medullary sinus; pMHCI, peptide-major histocompatibility class I; pMHCII, peptide-major histocompatibility class II.

Copyright © 2010 by The American Association of Immunologists, Inc. 0022-1767/10/\$16.00

DC cell levels entering the LN, pMHCII levels on DCs, and numbers of primed CD4+ T cell levels exiting the LN—can give us insight into the mechanisms that pathogens have evolved to evade the immune response at the level of CD4+ T cell priming.

A systems biology approach that incorporates *in silico* modeling to generate and test hypotheses, run virtual experiments, and make experimentally testable predictions is uniquely suited to address these questions. For example, modeling can be used to overcome the significant time scale (minutes to a few hours) and length scale (a few micrometers) limitations of 2PM experiments, allowing us to predict how the observed local cell behavior will translate into the behavior of an entire LN. Modeling can also enable prediction of the outcome of numerous and simultaneous processes in cases where it is too difficult to intuit the results. Specifically, agent-based models (ABMs) have been used in immunology and can allow an understanding of how local cell–cell interactions can lead to more global behavior (10, 15, 16, 20–27). We are interested in how individual DC and T cell contacts, binding, and proliferation events lead to generation of primed T cells, and how this outcome is affected by both immune and pathogen parameters. Compared with alternative approaches—such as cellular Potts model (17), cellular automata (28, 29), ordinary differential equations (30)—ABMs have unique advantages for modeling individual cell contacts. For a more complete discussion of ABMs, cellular automata, and other types of models as applied to biological systems, see two recent reviews (26, 31). ABMs can be used to simultaneously explore low frequencies of cognate T cells ($\sim 10^{-4}$ in this study), to track the history of each individual cell, to incorporate probabilistic events such as cell motion, and to follow the evolution of T cell priming in both space and time (15, 20). Furthermore, we have developed analytical tools both for uncertainty and sensitivity analysis and for assessing compensatory relationships (i.e., tradeoffs) between parameters (32). We have previously used an ABM to explore the representation of the detailed movement of T cells within the T zone of an LN via comparison of simulated motion and motion captured in 2PM studies (15). We now extend that framework to allow us to simulate physiologic or near-physiologic LN cell numbers and cognate frequencies over much longer time periods than 2PM studies capture, enabling us to both compare model results with infection scenarios and address some open questions regarding the dynamics of CD4+ T cell priming.

Materials and Methods

Agent-based model

ABMs are computational tools used to model behavior of a system resulting from interactions between individual components. ABMs consist of an environment, autonomous objects (agents), time steps, and rules governing the behavior of individual agents and interactions between agents. We implemented an ABM to simulate the immune response arising from cellular interactions within an LN (Fig. 1). This two-dimensional (2D) ABM accurately captures random encounters between T cells and DCs as observed via 2PM, with which it is possible to track individual cells as they interact with other cells and change their location and state (Fig. 1B). Previously, we developed an ABM that represented a small portion of an LN T zone and had sufficient spatial and time resolution to make observations at the level of individual cells (15). We found that chemotaxis-directed motion of T cells toward DCs increased the total number of contacts, but decreased unique contacts and thus inhibited efficient repertoire scanning of T cells, thereby decreased production of primed T cells. That is, our model supported the principle that a persistent random walk strategy of T cells to DCs was more efficient than chemotaxis-directed motion. [Persistent random walk implies that the cells do not turn back on the path they just came from, which is observed in 2PM studies (6–8).] In this study, we extend the scope of our LN ABM from a cellular level (fine grain) to a more biologically relevant histologic level (and coarser grain), that of the T zone.

Environment. We built a 2D model of the T zone of a LN. Compared with a three-dimensional model, our 2D model allows us to simulate an entire 2D slice of the T zone of an LN rather than just a small volume. Because our

goal was not to recapitulate and study cell movement, but rather to study the output of an LN during priming events, a 2D model is reasonable. Furthermore, for the parameter sensitivity studies contained herein, a model is required that can be used to run thousands of simulations in a reasonable amount of time. This is simply not yet possible with a three-dimensional model of the entire T zone of an LN or a reasonable portion thereof. Large numbers of cells are also required to study the relatively rare cognate CD4+ T cells on the simulation grid and generate statistically meaningful results, imposing a lower limit on the size of the LN model.

The environment of our model represents one complete slice of a whole T zone of a mouse LN (Fig. 1A). We chose to model the mouse rather than the human LN because more data are available for the mouse to test and validate our model. The dimensions of the T cell zone in a mouse LN are not available, but the volume can be reasonably assumed to be $\sim 25\%$ of the total LN volume of $\sim 1 \times 10^{-3} \text{ cm}^3$ (33). Thus, the T cell zone volume is $\sim 2.5 \times 10^{-4} \text{ cm}^3$. Our LN is represented by a 2D grid of 25×200 microcompartments (Figs. 1B, 4). The width and height of the T cell zone were matched to LN data as derived previously (15), particularly regarding the high endothelial venules (HEVs; entries) and medullary sinuses (exits). The thickness is set to one compartment. Each microcompartment is a $20\text{-}\mu\text{m} \times 20\text{-}\mu\text{m}$ square, yielding a T cell zone of $0.05 \text{ cm} \times 0.4 \text{ cm}$. Each microcompartment can hold one DC or up to four T cells. We assume that the field is one compartment deep, and thus the total volume simulated is $4 \times 10^{-5} \text{ cm}^3$. HEVs and afferent lymphatics are located toward the top of the grid, whereas medullary sinuses (MSs) that collect into the efferent lymphatics are located toward the bottom of the grid. These locations and distances between the HEV entrances and MS exits were established in our previous work, on experimental measurements from murine LNs, scaled appropriately to the new environment (15); recent work on mouse LNs agrees with our structural framework (33). Because our studies were not specifically aimed at understanding cell motion and movement, we did not include the fibroblastic reticular cell network within the LN in this model, although ongoing work in our group and others are considering this important structural component and its influence (17, 34).

Agents. Agents in our model are DCs, helper T cells (CD4+ cells), and effector T cells (CD8+ cells). Agents have attributes such as their unique identifier number (to track each individual cell), state (representing cell type), and location.

CD4+ T cells. CD4+ T cells are naive or primed. T cells are also either cognate (able to recognize Ag presented on MHC class II molecules on Ag-bearing DCs) or non-cognate. Only cognate cells can be primed.

DCs. DCs sample their environment and take up Ag to present on their surface (35). We assigned a pMHC level to each DC as it enters the grid. We represented a continuum of Ag-bearing DCs by tracking the quantity of peptide-MHC class complexes (pMHC) on the surface of DCs with time. DCs whose pMHCII value is below a threshold are incapable of priming naive, cognate CD4+ T cells and are designated as immature DCs (IDCs), and those capable of priming are designated as antigen-bearing DCs (Ab-DCs). The fraction of the DC population entering the LN that is Ag-bearing is varied in some of the simulations, and is referred to as *percent Ab-DCs*, but otherwise we assume that $\sim 60\%$ of all DCs are Ag-bearing as inferred from data (36). We also assume that the levels of pMHC on the surface and the numbers of Ab-DCs reflect the levels of Ag in a system, as previously described (10, 11). A third class of DCs (licensed DCs [LDCs]) have interacted with a primed CD4+ T cell and have increased numbers of pMHC (see below) (37, 38).

Cognate frequency. The frequency of cognate T cells is estimated to be on the order of $1:10^5$ to $1:10^6$ in actual infection scenarios (39, 40). In 2PM experiments in which is introduced by Ab-DCs that have been exposed to antigen (OVA), to increase the number of observable events during the time frame of an experiment, the frequency of cognate cells is enhanced to $\sim 1:300$ by using transgenic T cells and recipient mice (7). In our simulations, we vary the cognate frequency from $1:300$ to $1:10,000$. We are limited to a minimum frequency of $1:10,000$ to ensure that enough events occur during a simulation to allow statistical significance. This method allows us to predict how well the $1:300$ ratio represents other more biologically relevant scenarios.

T cell recruitment. Cognate and noncognate T cells enter the LN via HEVs. Rates of entry of T cells, their levels, and the ratio of CD4+ to CD8+ T cells were inferred based on the number of T cells present in a mouse LN (15) and the rate of their exit ($<24 \text{ h}$ for noncognate T cells) (4). See <http://malthus.micro.med.umich.edu/lab/movies/FullLN/> for more details. Recruitment rates via HEV allowed us to maintain the number of T cells in the LN at a steady state for the negative control simulations—that is, with no Ab-DCs present or entering the LN (data not shown). T cells leave the LN via the MSs that collect into efferent lymphatic vessels. In the simulation, they exit when they reach defined spots on the grid defined as MSs (Fig. 1B).

DC recruitment. DCs enter the LN via afferent lymphatics; estimates of the number of DCs are based on murine data (16). DC entry into the LN is

described via two distinct infection scenarios (see below). DCs are not allowed to leave the LN in our simulations, as this rarely occurs in the natural system.

CD8+ T cells. Although not the focus of this paper, the model also included CD8+ T cells (naive and primed). Naive CD8+ T cells can be activated by contact with an LDC only. Including these cells, which like CD4+ T cells can bind to a DC surface, ensures that we do not overestimate the available DC area available to CD4+ T cells. More detail on CD8+ T cells and the rules relevant to them can be found at <http://malthus.micro.med.umich.edu/lab/movies/FullLN/>.

Rules. ABM rules define individual cell behaviors such as cell motion, life span, changes of state, proliferation, and cell–cell interactions (Fig. 1B, 1C). A full set of rules is available at <http://malthus.micro.med.umich.edu/lab/movies/FullLN/>. Below we briefly describe key rules of our model that represent biologic mechanisms of key interest in this study.

Cell motion. Cells in our model follow a persistent random walk (Fig. 1B). Detailed data from 2PM tracking of individual T cell motion within an LN are available (7, 8, 41). Our model matches these data on cell speed, mean free path before changing direction, and cell motility (relationship between displacement and time from original tracking point; see <http://malthus.micro.med.umich.edu/lab/movies/FullLN/> for details on model validation). Similarly, data are available for validation of our model regarding DCs, which move more slowly, as do T cells that have become bound to a DC (7, 8). Our model also matches these data (15).

pMHC display. The $t_{1/2}$ of pMHCII complexes on IDCs is typically on the order of 24 h; however, Ag loaded onto MHC II molecules and presented on the surface of Ab-DCs (or LDCs) extends that $t_{1/2}$ to the lifespan of the cell itself (days) (12–14). In our simulations, pMHCII level is allowed to decrease according to a given $t_{1/2}$; we used a range of reported $t_{1/2}$ values for our analysis to determine the effects this parameter has on the system (36, 42, 43). As mentioned above, the $t_{1/2}$ of pMHCII is much shorter than that of pMHCII, although it may also be extended (12–14), and this affects the generation of primed CD8+ T cells. Because LDCs are efficient Ag presenters, we assume all the costimulatory molecules and pMHCII necessary are present for priming CD8+ T cells.

Contact. Contact between cells occurs when immune cells find themselves within the same or adjacent microcompartments (Fig. 1B). DCs use a strategy to allow rapid and efficient scanning of many T cells to locate the rare cognate T cell whose TCR has sufficient affinity with the pMHC on a DC to result in binding, priming, and proliferation of that T cell lineage. DCs may contact up to 5000 T cells per hour by moving their dendrites within a local “sweep area” (44, 45). We implemented this local sweep area by defining DC-T cell contact as a T cell occupying any of eight compartments adjacent to a DC, with a maximum of 32 simultaneous T-cell contacts per DC (because up to 4 T cells can fit into a micro-compartment). A range of 75–250 has been suggested in the literature (7, 44); thus, in 2D the value of 32 is reasonable.

Binding and priming of CD4+ T cells. Following physical contact between a CD4+ T cell and an Ab-DC or LDC, binding occurs only if both the quantity of pMHCII on the DC surface and the TCR affinity are sufficient (43), whereas priming requires prolonged binding duration (average of 6 h) and the minimum duration has been reported to vary inversely with pMHC level (11, 46) (Fig. 1C). Although data are scant, a sigmoidal relationship between T cell response and Ag dose on a DC has been described (47). Because not all DC-T cell binding leads to T cell priming, we separated binding and priming activities into two sigmoidal functions. Binding occurred with a probability determined by the pMHC level on the DC surface (Fig. 6); the parameters that characterize these curves are *binding threshold* and *binding shape*. Binding duration was determined by evaluating on an hourly basis whether pMHC level had decreased below a minimum threshold (because pMHC are lost over time)—termed the *unbinding threshold*. At the conclusion of binding, the product of binding duration and average pMHC level during the binding period is used as a priming signal to determine priming probability, based on a second sigmoidal function (Fig. 6). The parameters used to characterize this curve are *priming threshold* and *priming shape*. Additional factors also contribute to the ability of DC complexes to activate T cells, including affinity and kinetics of the association of pMHC with TCR and costimulation by other molecules (48–50), and are implicit in our representation in Fig. 6. For example, a weaker affinity or fewer costimulatory molecules would effectively move either or both curves in Fig. 6 to the right and/or down, whereas higher affinity or stronger costimulation would effectively move the curves left and/or up.

Proliferation. Primed CD4+ T cells proliferate based on a reported doubling time (eight hours) and average number of divisions is four (6).

Licensing of DC. Licensing of Ab-DCs can occur either by their contact with primed CD4+ T cells or by direct contact with an LDC via exosomes or exovesicles (51–53). In our model, we consider both mechanisms for licensing, each requiring only cell-to-cell contact (Fig. 1C). In

both cases, the state of the DC is changed to that of an LDC, and its pMHC level is increased to a level above the binding threshold (Fig. 6) to ensure enhanced ability for T cell priming.

Lifespan. Naive CD4+ T cells live up to 365 d (54). The age of a T cell entering the grid was chosen from a uniform distribution between 165 and 365 d. Primed CD4+ T cells and Ab-DCs have lifespans of 60 h (55). After becoming licensed, LDCs live for 36 h (56, 57).

Parameter estimation

All parameters and their values used in the ABM are listed in Table I (58–61). Parameters were based on experimental data or estimated based on related systems and the ability of the model to produce reasonable behavior (calibration) during a chronic infection scenario (see below and Fig. 2). Parameter values are expected to vary slightly from one cell to another; this is captured in the ABM by choosing parameters for each cell from a biologically reasonable defined range that is normally distributed. In addition, because there is uncertainty in the values of many of the parameters, it is important to examine closely the influence of parameter variation on the model outputs of interest, as described in the sensitivity analysis.

Virtual infection simulation

Both Ab-DCs and IDCs enter the LN; the entry of Ab-DCs simulates an infection. We considered two infection scenarios. The first, which we term the *acute infection scenario*, captures a multiday pulse of Ab-DCs entering the LN and the production of primed T cells that results. Our simulation is based on murine data (62) representing transport of Ag (FITC) from the airways to thoracic LNs via airway-derived CD11c⁺/MHC-II DCs (Fig. 2B). Transport of Ag by DCs begins within 6 h after introduction of FITC Ag into the airways, peaks after 24 h, and declines to zero by day 7. We used these data to infer the rate of entry of DCs (Fig. 2A; note that the cumulative number of DCs entering is shown).

We also considered a chronic infection scenario, an artificial construct to allow us to do a steady state analysis, thus avoiding confounding effects of changing numbers of Ab-DCs. In these simulations, we maintain a steady-state level of Ab-DCs post peak influx (~36 h) through day 14 of the simulation (Fig. 2E, 2F). This scenario was used for investigating the effect of varying cognate frequency and Ab-DC frequency.

For both infection scenarios, simulations are first run for 15 h to achieve a steady state of 5000 naive CD4+ and 4000 naive CD8+ T cells before infection. Infection is then introduced by adding DCs in a given ratio (termed % Ab-DCs) of IDCs and Ab-DCs (Fig. 2A).

Metrics used to analyze simulations

For each simulation, we track all properties for each cell (agent), including location (within the LN or exiting the LN). We use these data to compute the cumulative output of primed CD4+ T cells; cumulative refers to the summing of exiting cell numbers up to the time point plotted. In addition, we also compute three metrics to help us understand T cell–DC contact dynamics within the LN. *Search time* is defined as the time elapsed from when a cognate CD4+ T cell enters the LN until it first contacts an Ab-DC. *Transit time* is defined as the time required for a cognate T cell to migrate through the LN T zone, including any priming and division steps. *Match percentage* is defined as the percentage of entering cognate CD4+ T cells that contact an Ab-DC during their time in the LN.

Uncertainty and sensitivity analysis

Uncertainty analysis measures the variation in model output based on the variation of inputs (i.e., parameter values). Sensitivity analysis involves the correlation of these variances in parameter values to variances in model output and is particularly useful when parameter values are not known with certainty. We use Latin hypercube sampling (LHS) to sample from a large parameter space and partial rank correlation coefficients to determine sensitivity, as we previously described for application to ABMs (32). Parameters varied during sensitivity and uncertainty analysis are indicated in Table I, along with their default values, ranges tested, and references based on experimental data; this was done for acute infection scenario. In the LHS, the initial number of pMHC on the surface was not varied, because the parameters that describe all the binding and priming curves in Fig. 6 are sufficient to capture the effect without redundancy. If initial numbers of pMHC were included in the LHS/partial rank correlation coefficient, it would also show as an important parameter (data not shown) as observed in the trade-off plots.

Trade-off plots

We examined the relationship between two parameters, average initial numbers of pMHCII per Ab-DC entering the LN, and number of Ab-DCs as a percent of the total entering (which is fixed), in producing a fixed

number of primed CD4+ T cells during a chronic infection scenario. We used the chronic scenario so that varying levels of DCs would not effect the results. The distribution for initial levels of pMHC on the surface of the DCs was chosen from a much smaller range than the rest of the simulations, with a small SD of 5. An average of 10 runs were performed, and a target value of cumulative CD4+ T cells was achieved (100 for cognate frequency 1/3000 and 500 for cognate frequency 1/300) and the parameters yielding those values (within 10% of the target values) were obtained. These pairs of parameter values that yielded the same number of cumulative (14 d) primed CD4+ T cells leaving the LN were compiled and plotted. Because such plots yield information on how a change in one parameter can compensate for a change in the other parameter, we term these plots *trade-off plots* (48, 63).

History

We considered the scenario in which T cells retain memory of previous interactions with DCs, and this memory accumulates to assist in priming. We term this memory *history*. A control baseline condition had *no history*—that is, each T cell binding event is independent of prior contacts of that individual T cell, and T cell priming depends solely on its binding with a particular DC (all results shown in this article were done for this case). Second, we considered a scenario of binding sensitivity history for T cells in which prior binding events that did not lead to priming can increase the probability that a DC-T cell contact leads to successful binding. In this case, the pMHC value used to compute the binding probability (Fig. 6) is calculated by summing pMHC values from prior contacts (still decreasing with a given $t_{1/2}$). Finally, we considered the case of *priming sensitivity history*, in which prior T cell binding events (that failed to prime) increase the probability that subsequent binding events result in priming. In this case, the pMHC*duration values used to compute the priming probability (Fig. 6) are calculated by summing the pMHC*duration values from prior contacts (still

decreasing with a given $t_{1/2}$). Implementations of history were evaluated independently as well as a scenario in which priming and binding sensitivity occurred simultaneously.

Numerical methods and visualization

The ABM was implemented in C++. Code was developed on a Linux Mandriva 2007 operating system and compiled using a GCC compiler. The simulation time step was 6 s. To visualize results, we generated text files that record the state and location of every cell on the grid at 2 min intervals during the simulation. These text files were then converted to .png image files using Java 3D module (Sun Microsystems, Palo Alto, CA). Image frames were converted into movies using QuickTime Pro player (Apple Computer, Cupertino, CA). Movies of our ABM simulations are available at <http://malthus.micro.med.umich.edu/lab/movies/FullLN>.

Results

Viral infections track cell behavior and LN output of primed cells

To understand the dynamics of immune cells in the LN during both acute and chronic infections, we developed a computer model known as an ABM. DCs and naive T cells migrate to a single LN, interact according to a set of rules determined from known biological data, and T cells then leave the LN primed and ready to combat infection (Fig. 1). The cumulative number of primed CD4+ T cells exiting the LN via the MSs serves as a measure of the strength of the immune response generated for particular infection scenarios.

We first describe the dynamics of the acute infection scenario (Fig. 2A–D). Fig. 2A shows the cumulative number of DCs (60%

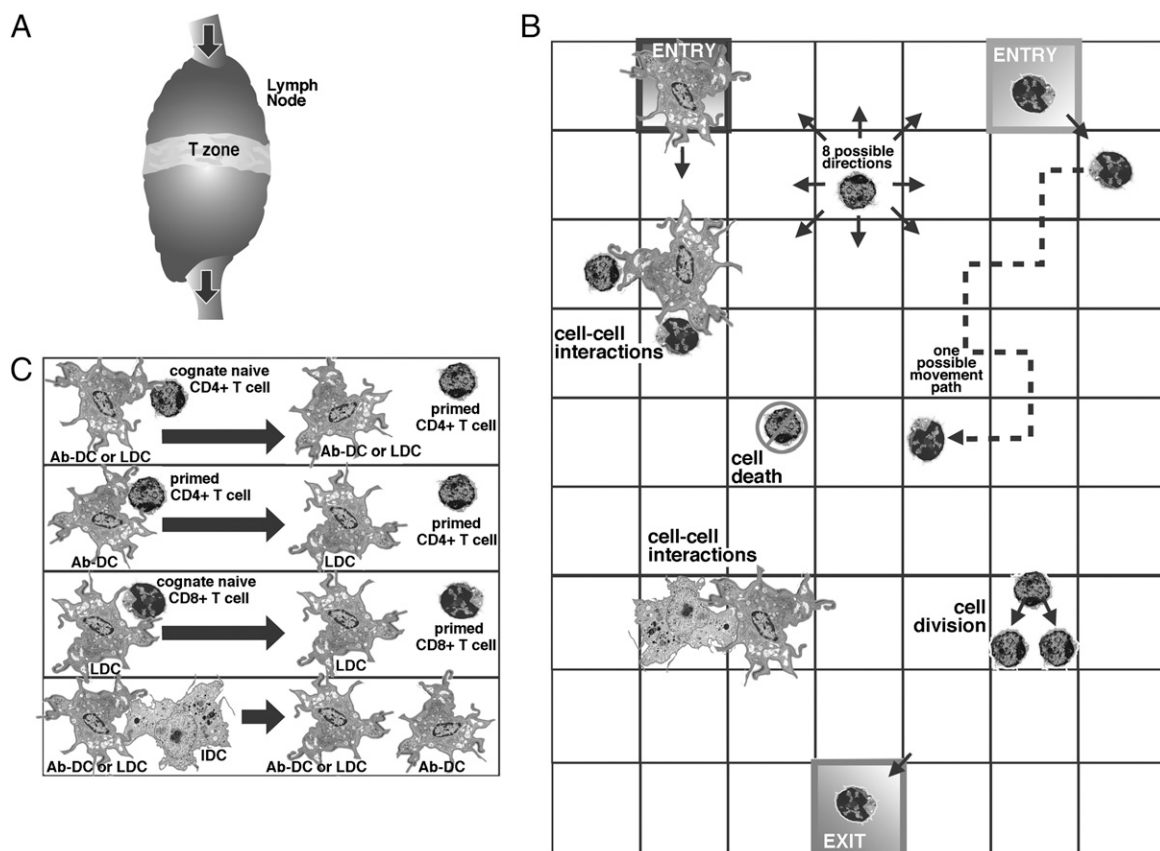


FIGURE 1. Model schematics and rules. *A*, The model represents events occurring in the T zone of the LN, a region in which naive T cells and DCs have an opportunity to interact. *B*, The model geometry is a section of LN represented by a lattice of 25×200 microcompartments, a section of which is diagrammed here. Cells move onto, off of, and around on the grid. T cells and DCs enter the grid via the high endothelial venules and afferent lymphatics, respectively. Cells can move to any adjacent square and can also divide. The larger DCs occupy an entire square, whereas up to 4 T cells (which are much smaller) can occupy a single square. Cells in adjacent squares can interact. T cells leave the grid via medullary sinuses that collect into efferent lymphatic vessels. *C*, Shown are possible cell–cell interactions. Interaction of an Ab-DC or LDC with a cognate naive CD4+ T cell can give rise to a primed CD4+ T cell (see also Fig. 6). Similarly, interaction of an LDC with a cognate naive CD8+ T cells can give rise to a primed CD8+ T cell. The interaction of an Ab-DC with a primed CD4+ T cell can produce an LDC, and the interaction of an Ab-DC or LDC with an IDC can produce an Ab-DC. Finally, LDCs can also license Ab-DCs.

Ab-DCs and 40% IDCs) that have entered the LN. The dynamics of all the DC populations in the LN are shown in Fig. 2B; the total DC population increases to a maximum of 100 by 36 h and then declines. Initially, the population of total DCs in the LN is composed of IDCs and Ab-DCs; as these DCs become licensed, the number of Ab-DCs declines and the number of LDCs increases. Although data are not knowledge available on the rate of entry of DCs into a draining LN, we can assume that for different infections, the dynamics of both timing and magnitude will be different. In this study, we chose the influx of DC dynamics to represent total numbers of DCs in the LN (the sum of Ab-DCs, LDCs, and IDCs) that represent experimentally determined values from one human study (Fig. 2B) (62). The cumulative predicted numbers of primed CD4+ and CD8+ T cells leaving the LN are shown in Fig. 2C and 2D. There are no data available on the number of CD4+ T cells leaving a single LN. However, a spleen is a secondary lymph organ, and there are data from one group looking at the expansion of cells during LCMV infection (64). The data show a 3 order-of-magnitude expansion in CD4+ T cell numbers and a 4 order-of-magnitude expansion in CD8+ T cell numbers over a 2 wk period. Our lymph node outputs (from just a portion of the LN) are similar. The magnitude and timing of the simulated expansion phase are similar to the data; the output from our simulated LN precedes that of the spleen data by a few days, as expected. Thus, our simulation captures essential features of an acute infection scenario in an LN. Time-lapse movies

of the acute infection scenario for two different cognate frequencies are available at <http://malthus.micro.med.edu/lab/movies/FullLN>.

For comparison with acute infection, we also simulated a chronic infection scenario (Fig. 2E–H). The entry of IDCs and Ab-DCs into the LN is set to reach a steady rate by ~1 d, as shown by a nearly constant rate of increase in the number of DCs that have entered the LN (Fig. 2E). In a manner similar to that seen for the acute case, the number of total DCs in the LN is initially composed of IDCs and Ab-DCs, but later switches to predominantly LDCs (Fig. 2F). The corresponding (cumulative) output of primed CD4+ and CD8+ T cells is shown in Fig. 2G and 2H. The cumulative cell numbers are initially similar to the acute case, but continue to increase slowly with time. Although this scenario is an artificial construct and not meant to be compared with experiment, chronic infection simulations will serve as a tool to observe the effects of varying the number of Ab-DC or cognate frequency without the confounding effect of varying levels of entering DCs.

T cells can potentially contact multiple DCs during their transit through an LN. The extent to which separate contacts might lead to subsequent priming and proliferation has been previously studied in models of CD8+ T cell priming (11, 46, 65). To explore whether previous contacts between naive CD4+ T cells and DCs influence CD4+ T cell binding and/or priming, we implemented various history scenarios (see *Materials and Methods*; binding sensitivity history, priming sensitivity history, and the sum of the

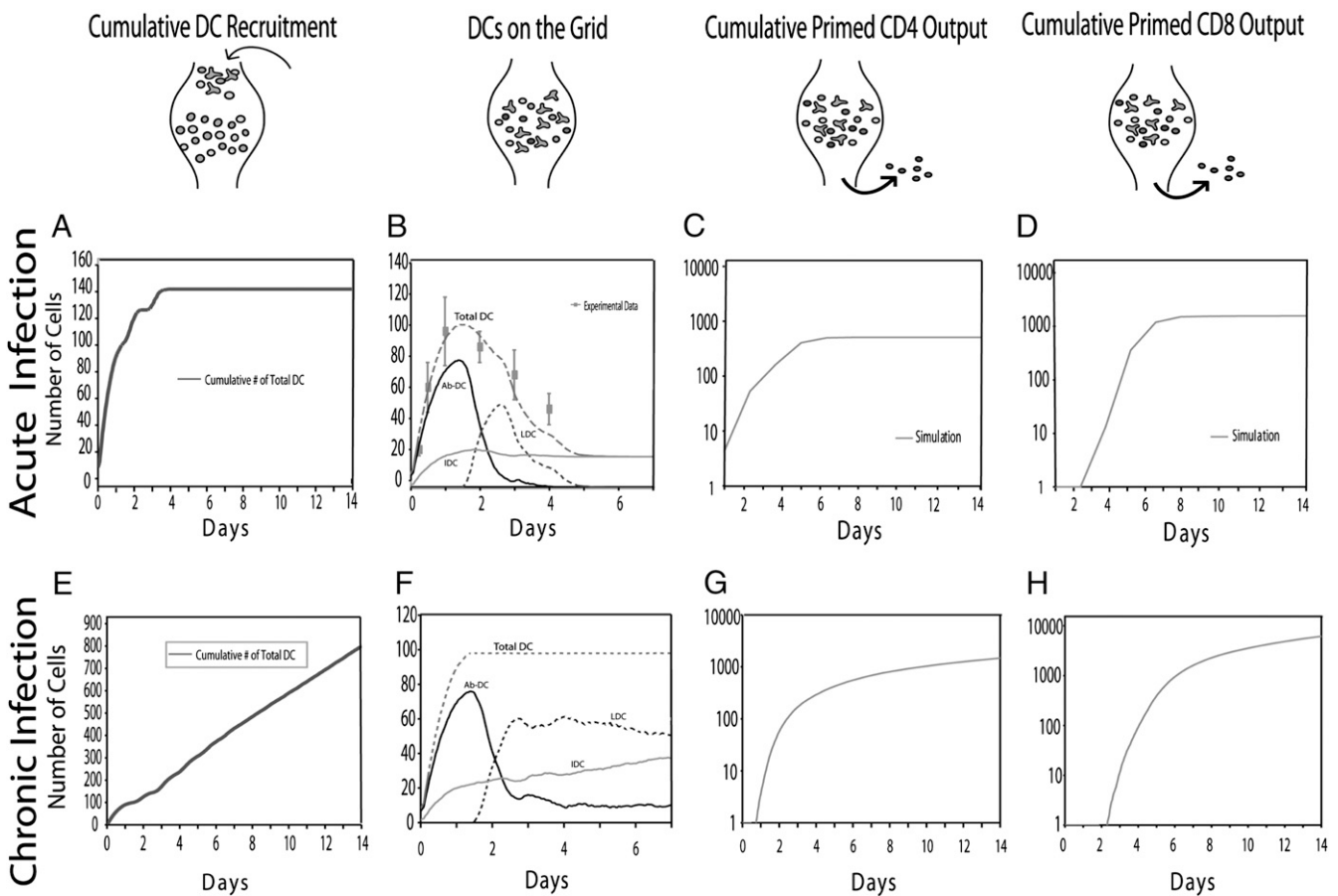


FIGURE 2. Acute and chronic infection scenarios. The cartoons along the top indicate the flow of cells into, on, and out of the LN and correspond to the plots below. *A* and *E*, Cumulative number of DCs that have entered the LN. *B* and *F*, Numbers of each population of DCs in the LN during the infection. In *B*, experimental data on the total number of DCs in a human LN at particular times (66) is shown for comparison. *C* and *G*, Cumulative number of primed CD4+ T cells exiting the LN. *D* and *H*, Cumulative number of primed CD8+ T cells exiting the LN. In *C* and *D*, experimental data from a mouse spleen are shown for comparison (64). No measure of variability (e.g., SD) is available for these data. Model parameter values used are from Table I with 60% Ab-DCs, cognate frequency 1:300, pMHC $t_{1/2}$ of 60 h.

two). We set the “memory” of these contacts to decay with a similar time-frame as pMHC themselves are lost (60 h $t_{1/2}$). We found no significant differences in generation of primed CD4+ T cells when we performed the experiments in any of the history cases versus no history control (<http://malthus.micro.med.umich.edu/lab/movies/FullLN/>). This finding provides a strong argument that, at least for priming of CD4+ T cells, this concept of history may not be playing a significant role in the generation of primed CD4+ T cells that leave the LN. We note that if the pMHCII $t_{1/2}$ is reduced by an order of magnitude to that of pMHCI, we do find an effect of history, in agreement with previous work by Zheng et al. (10) on the priming of CD8+ T cells.

LN efficiency in producing primed CD4+ T cells is primarily a function of the number of Ab-DCs

The influx of Ab-DCs and cognate CD4+ T cells to an LN is central to the generation of primed T cells; however, the relationship between the numbers of Ab-DCs and cognate T cells entering an LN and primed CD4+ T cells generated and exiting an LN is not known. We investigated a range of cognate frequencies, from the elevated frequency (1:300) typical of 2PM experiments to a frequency approaching physiological (1:10,000). Similarly, we varied the fraction of entering DCs carrying sufficient levels of Ag to

prime a T cell (percent Ab-DCs). Under basal conditions, DCs represent <1% of cells within LNs (15, 66); infections likely generate increased and varying levels of Ab-DCs. To study the influence of these inputs on primed CD4+ T cell production, we used the chronic infection scenario (Fig. 2).

Fig. 3A shows the simulation of cumulative output (through day 14) of primed CD4+ T cells from an LN for five different cognate frequencies and a range of percent Ab-DCs. For a given cognate frequency, increasing the percent Ab-DC increases the cumulative output of primed CD4+ T cell, as expected. Similarly, for a given percent Ab-DC, increasing the cognate frequency increases the output of cumulative primed CD4+ T cell.

To determine whether the LN efficiency (i.e., the generation of primed T cells leaving the LN) varies with cognate frequency or percent Ab-DC, we plotted the ratio of the cumulative primed CD4+ T cell output to the number of naive cognate CD4+ T cells entering the LN (primed CD4/cognate CD4 T cell; Fig. 3B). As the percent Ab-DCs is increased, a saturation effect is observed; this is anticipated because DCs can act catalytically—that is, one DC can activate more than one T cell. The curves for each cognate frequency fall almost on top of each other, indicating that LN efficiency is nearly independent of cognate frequency. The separation between the curves in Fig. 3B at low values of percent Ab-DC suggests that

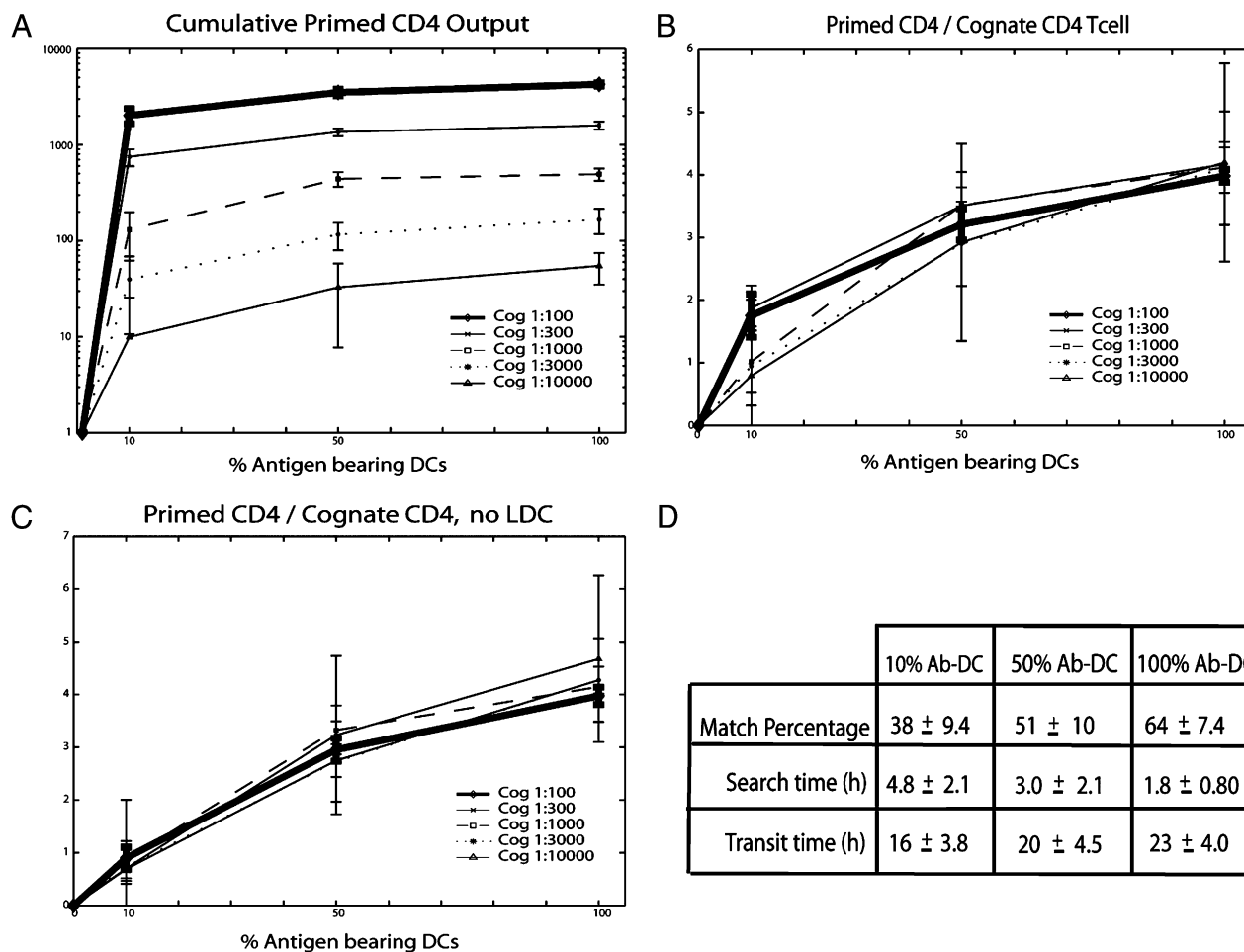


FIGURE 3. Simulation of primed CD4+ T cell production during chronic infection (i.e., input of DCs is constant). *A*, Cumulative (14 d) output of primed CD4+ T cells from the LN as a function of percent Ab-DC by differing cognate frequencies (Cog). *B*, Data in *A* replotted as the ratio of the cumulative primed CD4+ T cell output to the number of naive cognate CD4+ T cells entering the LN for different cognate frequencies. (The numbers are nearly identical if you use data from the simulations used to construct *C*.) *C*, Simulations results as in *B*, but for no licensing of DCs. *D*, Average match percentage, search time and transit time for cognate CD4+ T cells entering the LN for the simulations shown in *A* and *B*. Standard deviations are also given. Data in *D* are averaged across all cognate frequencies, because differences between cognate frequency were not statistically significant for these outputs. Simulation parameter values are found in Table I.

there is a slight effect of cognate frequency on the output of primed CD4+ T cells per cognate CD4+ T cell entering the LN. This effect is due to the positive feedback provided by LDCs: primed CD4+ T cells interact with Ab-DCs, leading to production of LDCs which, by virtue of their higher pMHC levels, are efficient activators of CD4+ T cells. This is apparent only at low values of percent Ab-DCs, where contact between T cells and DCs is less frequent. When we remove the pathway leading to LDC production, the data show no significant effect of cognate frequency on the ratio plot (Fig. 3C).

Our finding that LN efficiency is nearly independent of cognate frequency is consistent with the data (67) showing that CD4+ T cell populations expanded in proportion to their naive progenitors. Thus, increasing the percent Ab-DC increases the likelihood that a naive T cell will meet its DC match, but changing the cognate frequency has no effect on LN efficiency. Although there is certainly some crowding on the grid (Fig. 4), we do not find that Ab-DCs are always completely surrounded by cognate T cells and thus unable to activate additional T cells. The evidence for this finding is that as the cognate CD4+ T cell frequency is increased, approximately the same percentage of T cells become activated (Fig. 3B). Fig. 3B also provides a quick assessment of the function of the LN in priming CD4+ T cells, in that for physiologically realistic values of the numbers of entering Ab-DCs during an infection, on the order of 1–4 primed CD4+ T cells will be produced for every cognate CD4+ T cell entering the LN.

We pooled the data from the simulations shown in Fig. 3B to calculate the average match percentage, search time, and transit time for cognate CD4+ T cells entering the LN (Fig. 3D). As the percent Ab-DCs increases, more CD4+ T cells are able to find

their DC match, and more quickly, by random walk. Transit times increase with percent Ab-DC because many T cells are now binding to DCs for several hours on their path through the LN. These transit times are consistent with data from whole animal experiments (68).

The calculated quantities from Fig. 3D can help us to understand the values of the ratio-primed CD4/cognate CD4 T cell in Fig. 3B. For example, note that at 50% Ab-DCs, approximately half of the naive cognate CD4+ T cells find their DC match. Those T cells take an average of 3 h to find their DC match and after binding have time for two to three divisions. The other half of the T cells do not find a match, and thus the primed CD4+/cognate CD4+ T cell ratio of ~ 3 reflects that a significant part of the population of entering T cells do not contribute to generation of primed CD4+ T cells leaving the LN.

Peptide-MHC levels and numbers of Ag-bearing dendritic cells trade off to give similar levels of T cell output

There are two key parameters that characterize the role of the Ab-DC in CD4+ T cell priming: the number of Ab-DCs that enter and the ability of each to successfully prime CD4+ T cells as quantified in this study by pMHCII levels. Together, these parameters serve as a measure of the Ag in the system. To determine whether these parameters play equivalent roles (i.e., whether a deficiency in the number of Ab-DCs can be overcome by introducing only Ab-DCs with high levels of pMHCII) we performed simulation experiments with our ABM. Pairs of values of pMHCII and percent Ab-DC that gave similar cumulative (14 d) numbers of primed CD4+ T cells exiting the LN were plotted (Fig. 5). These plots demonstrate that efficiency in one process (e.g., the display of many pMHCII by

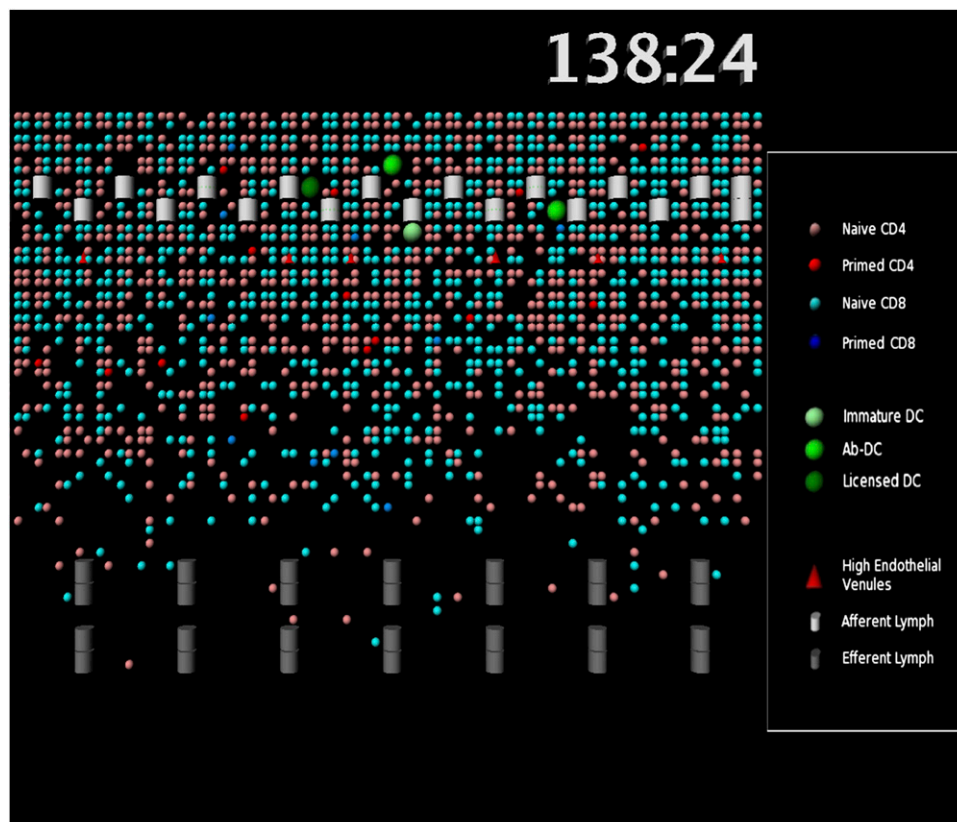


FIGURE 4. Simulation snapshots. An enlarged view of a portion of the LN simulation grid is shown. High endothelial venules (red triangles), afferent lymphatics (white cylinders), and medullary sinuses (gray cylinders) are indicated; these are the entrance and exit ports for cells. Individual cells are shown as circles of various colors. See legend for details. 138:24 represents the time the snapshot was taken in hours and minutes.

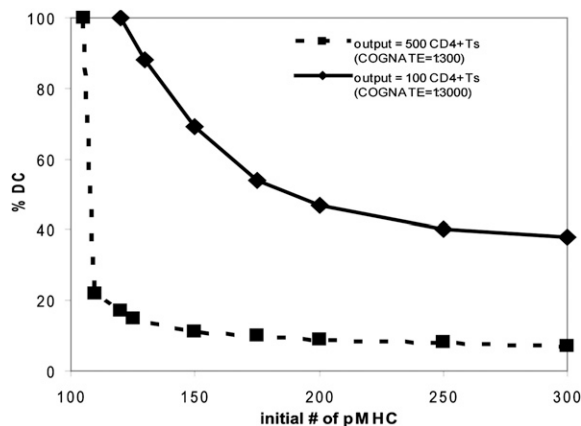


FIGURE 5. Trade-off between initial pMHC levels on DCs and percent Ab-DC affect primed CD4+ T cell production. Pairs of values of the percent Ab-DCs and the number of pMHCII per Ab-DC that gave the same cumulative (14 d) output of primed CD4+ T cells are plotted. Cognate frequency 1:3000 (100 cumulative primed CD4+ T cells at day 14, solid line) and cognate frequency 1:300 (500 cumulative primed CD4+ T cells at day 14, dashed line) are shown.

each Ab-DC) can compensate for a deficiency in the other process (e.g., entry of Ab-DCs into the LN). Interestingly, the slopes of the trade-off curves for two different cognate frequencies (1:300 versus 1:3000) are different. At high cognate frequency (1:300), many cognate CD4+ T cells are present. Opportunities for multiple T-DC contacts mean that, once a minimum number of pMHC are present on the Ab-DC (~110 pMHC), there are sufficient opportunities for T cell activation, even given the low probabilities of binding and priming implied (Fig. 6). However, at low cognate frequency (1:3000), there are fewer opportunities for DC-T cell contacting, allowing the DC parameters (percent DCs, pMHC levels) to play equivalent roles (indicated by the less steep slope of the trade-off curve). This trade-off between percent Ab-DCs and levels of pMHC has also been observed for CD8+ T cells as well, although they showed that pMHC concentration is more important, as expected because the $t_{1/2}$ of pMHC I is much less than for the pMHC II in this study (10, 11).

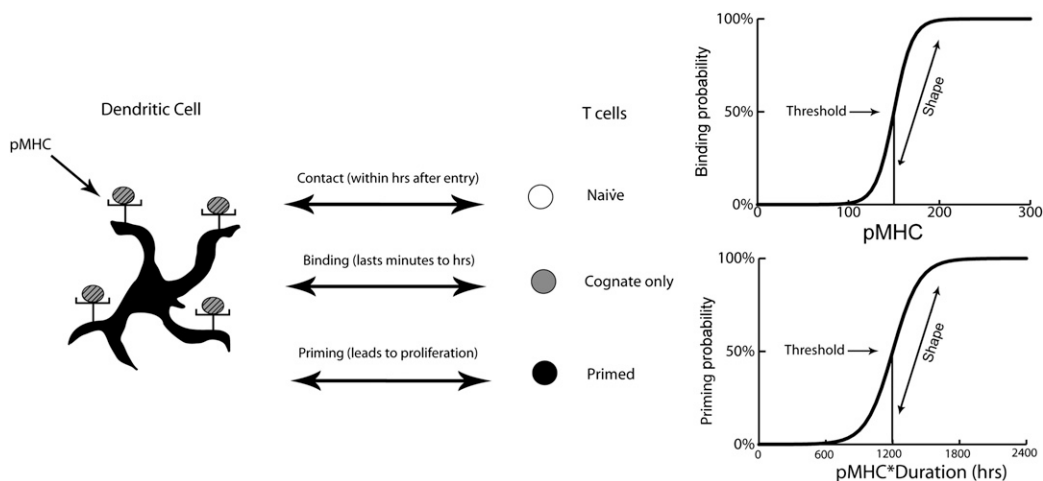


FIGURE 6. Interaction of an Ab-DC with a cognate naive T CD4+ cell can result in binding and priming of a T cell. Shown are the sigmoidal relationships used in the model (more details and equations are given at <http://malthus.micro.med.umich.edu/lab/movies/FullLN/>). Binding probability is assumed to be a function of the number of pMHCII displayed by the Ab-DC; the curve is characterized by the binding threshold and binding shape parameters. Binding threshold defines the number of pMHCII at which the binding probability is 50%; binding shape describes the slope of the binding probability versus pMHCII level curve at that point. Priming (of a CD4+ T cell already bound to an Ab-DC) is assumed to be a function of the product of pMHCII and time; the curve is characterized by the priming threshold and priming shape parameters.

Identification of key mechanisms that control LN output of primed CD4+ T cells

Our analysis up to this point has focused on the effect of varying the numbers of entering cells (cognate frequency, Ab-DC frequency) and the quality of those cells (pMHC number on an Ab-DC) on the LN output of primed CD4+ T cells. However, parameters that describe the efficiency and kinetics of various processes that occur within the LN also play an important role in generating primed CD4+ T cells. To identify key parameters and processes, we performed a model sensitivity analysis using a technique that allows multiple parameters to be simultaneously varied over physiologically reasonable ranges (see *Materials and Methods* and <http://malthus.micro.med.umich.edu/lab/movies/FullLN/>). When model parameters were simultaneously varied (parameters 1–16 in Table I), sensitivity analysis identified four parameters that have the strongest influence on the generation of primed CD4+ T cells (Table II, Tier 1 Parameters). As expected from earlier results (Fig. 3), these parameters include both cognate frequency and Ab-DC frequency. The maximum number of divisions a primed cell can undergo is also significantly and positively correlated with LN output. The time it takes for a T cell to divide (division time) is significantly but negatively correlated with LN output. Note that these tier 1 parameters identified by sensitivity analysis can be classified as either inputs into the LN or cellular properties that at first glance appear unrelated to DC-T cell interactions and more related to cell physiology.

To determine whether parameters describing DC-T cell interactions also significantly influence the LN output, but perhaps at a more subtle level than the tier 1 parameters, we performed a second sensitivity analysis fixing the tier 1 parameters at biologically relevant values, but allowing all other model parameters to vary over physiologically reasonable ranges (Table I). In this way, we identified four additional parameters that have a significant effect on the generation of primed CD4+ T cells exiting the LN (Table II, Tier 2 Parameters). The tier 2 parameters identified are all related directly to the interactions of the DCs and T cells in the LN. Recall from Fig. 6 that the binding and priming thresholds determine the probability that a particular Ab-DC (or LDC) is able to bind and ultimately prime a cognate T cell. Both the binding and priming thresholds are negatively correlated with primed CD4+ T cell output, because increasing either threshold lowers the probability

Table I. All parameters used in ABM simulations

	Parameter	Baseline Value	Range	Description	
+	1	pMHC half-life	60 h (58)	30–60 h	Half-life of pMHCII on DC
+	2	Unbinding threshold	100	80–120	pMHC level at which T cell unbinds from DC
+	3	Binding threshold	150 (59, 60)	100–200	pMHCII level corresponding to 50% CD4+ T cell binding probability
+	4	Binding shape	15	10–30	Shape parameter for CD4+ T cell binding probability curve (Fig. 6)
+	5	Priming threshold	6 h (46)	4–8 h	Value of pMHC*binding duration at 50% CD4+ T cell priming probability
+	6	Priming shape	0.6	0.3–0.9	Shape parameter for CD4+ T cell priming probability curve (Fig. 6)
+	7	Binding threshold (CD8 cell)	200 (11)	100–200	pMHCII level corresponding to 50% CD8+ T cell binding probability
+	8	Binding shape (CD8 cell)	15	10–30	Shape parameter for CD8+ T cell binding probability curve (Fig. 6)
+	9	Priming threshold (CD8 cell)	6 h	4–8 h	Value of pMHC*binding duration at 50% CD8+ T cells priming probability
+	10	Priming shape (CD8 cell)	0.6	0.3–0.9	Shape parameter for CD8+ T cell priming probability curve (Fig. 6)
+	11	LDC lifespan	36 h (56, 57)	24–48 h	Lifespan of an LDC
+	12	Prob T4 licenses Ab-DC	50%	30–80%	Probability of primed CD4+ T cell licensing Ab-DC
+	13	Cognate frequency	0.25 (see text)	1:100–1:10,000	Frequency of cognate naive T cells
+	14	Ab-DC lifespan	60 h (61)	40–80 h	Lifespan of an Ab-DC
+	15a	Number of divisions primed CD4+ T cells	4 (7, 58)	2–8	Maximum no. of divisions allowed for a primed T cell
	15b	Number of divisions CD8+ T cells	8 (7)	2–12	Maximum no. of divisions allowed for a primed T cell
+	16	Division time	8 h	2–16 h	Time for primed CD4/CD8 division
	17	Prob_T4_recruitment	99%	50–100%	Probability of naive CD4+ T cell recruitment at every 20 time steps
	18	Prob_T8_recruitment	95%	50–100%	Probability of naive CD8 recruitment at every 20 time steps
	19	Initial_naiveT4_cells	6000		Initial no. of naive CD4+ T cells
	20	Initial_primedT4_cells	0		Initial no. of primed CD4+ T cells
	21	Initial_naiveT8_cells	5000		Initial no. of naive CD8+ T cells
	22	Initial_primedT8_cells	0		Initial no. of primed CD8+ T cells
	23	Initial_total DCs_cells	8		Initial no. of total DCs (IDC+Ab-DC)
	24	% Ab-DCs	60%		Percent of total DCs that are Ag bearing
	25	Peak_DCs_level	100		Maximum no. of total DCs on the grid
	26	IDC_Ab-DC_threshold	50		pMHC level below which a DC is IDC
	27	n_tcells_bind_DC	32		Maximum no. of T cells that bind to a DC
	28	max_time_T4_primed	60 h (55)		Maximum time after which primed T4 cells die
	29	max_time_T8_primed	60 h (55)		Maximum time after which primed T8 cells die
	30	min_T4cell_age	165 d (54)		Minimum age of naive T4 when it appears on the grid
	31	max_T4cell_age	365 d (54)		Maximum age of naive T4 when it appears on the grid
	32	min_T8cell_age	165 d (54)		Minimum age of naive T8 when it appears on the grid
	33	max_T8cell_age	365 d (54)		Maximum age of naive T8 when it appears on the grid
	34	min_DC_age	24 h (61)		Minimum age of DC when it appears on the grid
	35	max_DC_age	11 d (61)		Maximum age of DC when it appears on the grid
	36	Initial number of pMHC	Taken from a distribution (59, 60)	125–200	Initial number of pMHC placed on surface of DC

For each parameter, the name, brief description, baseline value, and range used for uncertainty and sensitivity analysis is given. Parameter values are based on experimental data or estimated based on related systems and the ability of the model to produce reasonable behavior (calibration) during a chronic infection scenario. For example, recruitment parameters *prob_T4_recruitment* and *prob_T8_recruitment* were fixed to achieve a normal level steady state in the system before infection was introduced. T4, CD4+ T cells; T8, CD8+ T cells. *Parameters included in 16 parameter (full) LHS. *Parameters included in 12 parameter LHS.

that a T cell will be primed. Similarly, the unbinding threshold is negatively correlated with primed T cell output. At low cognate frequencies (1:3000; Table II), these three tier 2 parameters lose significance, indicating that there are differences between dynamics at different cognate frequencies. For a more detailed discussion, see <http://malthus.micro.med.umich.edu/lab/movies/FullLN/>.

Finally, of the tier 2 parameters, pMHC $t_{1/2}$ is strongly correlated with primed CD4+ T cell generation and exits from the LN at both cognate frequencies. This means that, if the pMHCII complexes are short-lived (the lower end of the range we tested was 30 h), there is a significant reduction in the generation of primed CD4+ T cells. However, it is well-documented that Ab-DCs (and similarly LDCs) can extend the $t_{1/2}$ of the pMHCII complexes on the surface to beyond the lifespan of the DC (12–14, 69). This mechanism is evolutionarily beneficial, because extending the $t_{1/2}$ of pMHC allows for continual

priming of cognate T cells by DCs. Kinetic stability of pMHCII complexes has also been found to be a key parameter of immunodominance, as complexes with a $t_{1/2} < 10$ h were usually cryptic, whereas dominant immune peptides had a long $t_{1/2} (> 150$ h) (69, 70).

Detailed results of our sensitivity analyses are given at <http://malthus.micro.med.umich.edu/lab/movies/FullLN/>. We also note that model parameters not identified as tier 1 or tier 2 parameters can still affect LN outcome, but not as significantly, at least within the ranges tested.

Identification of pathogen-affected processes that may influence generation of primed CD4+ T cells

Pathogens are known to interfere with the immune system via several mechanisms that affect DC–T cell interactions in the LN. If the biologic mechanisms identified in the sensitivity analysis (see previous

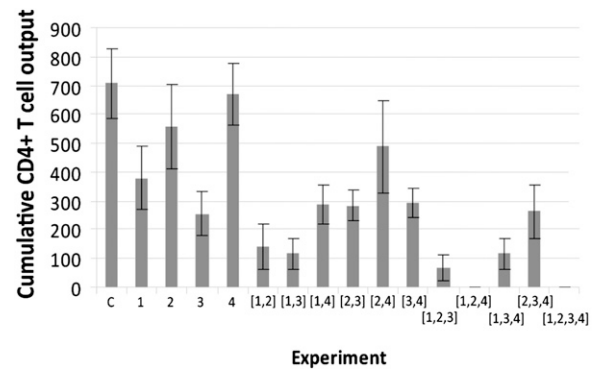
Table II. Results of model sensitivity analysis

Parameter	+/- Correlation	
	1:300	1:3000
Tier 1		
Cognate frequency	-	
Number of divisions	+	
Division time	-	
Percent Ab-DC	+	
Tier 2		
pMHC $t_{1/2}$	+	+
Unbinding threshold	-	
Binding threshold	-	
Priming threshold	-	

Tier 1 parameters are those identified as the most significant factors affecting the cumulative (14 d) output of primed CD4+ T cells when 16 of the model parameters (from Table I) are varied (<http://malthus.micro.med.umich.edu/lab/movies/FullLN/> and data not shown). Tier 2 parameters are identified as significant when 12 parameters from Table I are varied. Results are listed for two sample cognate frequencies, 1:300 and 1:3000. See <http://malthus.micro.med.umich.edu/lab/movies/FullLN/> for details. All values shown are $p < 0.01$.

section) were targets with which pathogens evolved to interfere during infection, would the generation of primed CD4+ T cells be effected? To explore this further, we simulated these “pathogen affects” on DC-T cell interactions by choosing four key mechanisms known to have an effect on primed CD4+ T cell generation, as identified in the sensitivity analysis (Table II): pMHCII $t_{1/2}$, unbinding threshold, binding threshold, and priming threshold. Although it is known that pathogens can affect aspects of immune system function, the extent to which individual mechanisms influence LN output of primed CD4+ T cells is unknown and not possible to quantify experimentally. To simulate these pathogen-related factors, we reduced (or increased) the mechanism under study by a standardized amount to observe the effects these changes have on the output of primed CD4+ T cells. We did this not only for each parameter independently, but also for the four chosen mechanisms (parameters) in different combinations.

Fig. 7 shows the cumulative (14 d) totals for primed CD4+ T cells leaving the LN. Our results show that changes in the values for each of the four mechanisms (parameters) individually reduce the output of both primed CD4+ T cells. It is interesting to consider whether pathogens would adopt a strategy that affects only a single process in the DC-T cell interaction, but what if pathogens evolved to affect multiple processes simultaneously? We explored this possibility by first combining effects to the four processes in groups of two. The overall effect on primed CD4+ T cell output can be both greater than or less than the sum of the two processes acting individually. For example, when we affect both pMHC $t_{1/2}$ and the unbinding threshold (processes 1 and 2 in Fig. 7), we get a greater than additive affect. However, when both pMHC $t_{1/2}$ and the binding threshold (processes 1 and 3 in Fig. 7) are affected, we get a less than additive effect, on average. This finding follows from the nonlinear relationship between binding and priming parameters (Fig. 6). We can also consider a pathogen affecting three or four processes simultaneously. When mechanisms 1, 2, and 4 are simultaneously pathogen-affected, the generation of primed T cells is completely abrogated. This suggests that a synergy exists between the mechanisms operating during DC-T cell dynamics that, if disrupted, leads to a dramatic effect. Our result provides a strong argument for selection of pathogens that can interfere with multiple elements of DC-T cell interaction dynamics. In other words, a pathogen that can reduce the numbers of pMHCII (perhaps by reducing pMHC $t_{1/2}$) and in addition can shift the binding threshold, priming threshold, or unbinding threshold (Fig. 6; perhaps by affecting costimulatory molecules) should be more successful than a pathogen that affects only one of these mechanisms.



Parameter #	Parameter	Base line value	Value changed to
1	pMHC halflife	36	10
2	Unbinding threshold	100	180
3	Binding threshold	150	300
4	Priming threshold	6	12

Experiment label	Parameters varied
C	None
1	1
2	2
3	3
4	4
[1,2]	1 and 2
[1,3]	1 and 3
[1,4]	1 and 4
[2,3]	2 and 3
[2,4]	2 and 4
[3,4]	3 and 4
[1,2,3]	1, 2 and 3
[1,2,4]	1, 2 and 4
[1,3,4]	1, 3 and 4
[2,3,4]	2, 3 and 4
[1,2,3,4]	1, 2, 3, and 4

FIGURE 7. Effect of inhibition of particular mechanisms on primed CD4+ T cell output. Cumulative (14 d) CD4+ T cell output (cognate frequency 1:300) from the LN is shown for 1) reduced pMHC $t_{1/2}$, 2) increased unbinding threshold, 3) increased binding threshold, and 4) increased priming threshold. Each parameter was reduced (or increased) by a standardized amount (lowest or highest range value and then by half as much more reduced (or added)). The effect of combinations 2, 3, and 4 is also shown.

Discussion

Generation of an adaptive immune response begins with physical encounters between Ab-DCs and T cells whose receptors have high affinity for a specific peptide-MHC complex. Trafficking of T cells and DCs into the LN leads to multiple opportunities for contact between Ab-DCs and cognate T cells. Unfortunately, many of the fundamental processes and parameters that describe the functioning of an LN are difficult to measure experimentally. For example, 2PM studies are by necessity limited to small areas of observation (micrometers) and short times frames (minutes to only a few hours). Most significantly, the relationship between Ag dose (in terms of density of Ab-DCs or how laden individual DCs are with Ag), frequency of matching cognate T cells, and generation of primed CD4+ T cells are not known. Many of these questions have been recently explored for CD8+ T cells (10, 11), but they remain open for CD4+ T cells. In addition, experimental protocols to investigate such phenomena often involve infusion of cognate T cell clones or introduction of large numbers of DCs, both necessary for measurable results, but often outside the usual biologic range of cell frequency or density (9). There is often an underlying assumption of proportionality, either explicitly stated in models or implicitly understood while interpreting results. For example, one might assume that if the density of Ab-DCs were reduced to 10 or 1% of the original amount, then the output would be proportionately reduced, but this is currently an open question. The implications of these relationships are important for understanding the roles that pathogens, pharmaceutical interventions, and vaccines can have on the immune response.

In this study, we develop a 2D computational model of a complete T cell zone of an LN and its ability to generate primed CD4+ T cells, and we use it to simulate the dynamics of immune cell interactions in an LN during a virtual infection (Fig. 2) over long time frames (days). The timing and the magnitude of the generation of primed CD4+ and CD8+ T cells are consistent with the scant data available, with more primed CD8+ than CD4+ T cells generated (64). Thus, these simulations provide a first look at how infection (characterized by the introduction of Ab-DCs into the LN) translates into generation of primed CD4+ T cells exiting from a single LN.

Our model allows us to quantify the relationship between cognate frequency and total number of primed T cells leaving the LN over a 14 d period. Interestingly, generation and output of primed CD4+ T cells from an LN scales with naive cognate CD4+ T cell input for a fixed Ab-DC level, with a small, positive feedback effect from the LDC pathway (Fig. 3) and one to four primed CD4+ T cells produced per entering naive cognate CD4+ T cell.

We can also quantify the relationship between Ag dose and generation of primed CD4+ T cells by the LN. Ag dose is composed of two different factors: how many Ab-DCs enter the LN and how many pMHCs are present on the surface of these Ab-DCs (11). Increasing either the number of Ab-DC or the number of pMHC on those Ab-DCs increases the output of primed CD4+ T cells, as expected (Figs. 3, 5). This can be visualized as a trade-off (Fig. 5) between the number of Ab-DC and their ability to present Ag. High numbers of Ab-DCs can compensate for low values of pMHC, and vice versa.

One wonders whether the 2PM experiments with their necessarily high cognate frequency and high numbers of Ab-DCs can give insight into a more physiologic lower frequency situation. Because extrapolation of results to situations outside the range of an experiment is fraught with error, supplementation of experimental results with the *in silico* simulations is useful. Thus, our results suggest how to extrapolate results obtained using 2PM to understand actual infection dynamics: the output of primed CD4+ T cells scales linearly with cognate frequency, but nonlinearly with the number of Ab-DCs present (Fig. 3).

Physiologic cognate frequency is not known definitively, but recent estimates in mouse (67), suggest ~20–200 cognate naive CD4+ T cells out of a total population of 10^7 , thus giving an estimate of cognate of $1:10^5$; if one considers multiple epitopes from a single Ag being presented by a single DC, one can imagine that the effective cognate frequency is increased by an order of magnitude (i.e., $1:10^4$). We are able to consider in our model cognate frequencies as low as $1:10^4$. Unfortunately, estimates of the number of Ab-DCs present in an actual infection are scarce. The number of Ab-DCs tested in this study is consistent with the scant data available, but more data are needed on this point.

Our simulations offer interesting and novel statistics on the passage of a cognate T cell through an LN (Fig. 3). The number of CD4+ T cells that find their DC match is significantly less than 100%, even at the numbers of Ab-DCs tested in this study, which are likely at the high end of the true physiologic range. CD4+ T cells require ~2–5 h to find their DC match and 16–23 h to transit through the LN, consistent with an earlier calculation for a smaller section of an LN (15) and experimental (i.e., 2PM) data (6–8).

Our analysis allows us to quantify the degree to which mechanisms that are part of the DC–T cell interactions contribute to the generation of primed CD4+ T cells (Fig. 7; Table II; <http://malthus.micro.med.umich.edu/lab/movies/FULLLN/>). Interestingly, these factors are precisely those that pathogens have been identified to inhibit. Microbes are known to alter DC–T cell interactions in multiple and even overlapping ways. Data support the effects of both bacteria and viruses on DC recruitment, maturation, and survival. Herpes virus and poxvirus can encode homo-

logs of chemokine receptors that function as chemokine antagonists and prevent recruitment of additional DCs to the site of an infection (18, 19). *Shigella* and *Salmonella sp.* can activate DC apoptosis via caspase 1 (71, 72). Vaccinia can inhibit DC maturation and induce DC death by apoptosis (73). Inhibition of DC maturation has been shown to occur via 1) secretion of altered receptors that block interferon, TNF- α , or IL-1; 2) secretion of regulatory cytokines such as viral IL-10s from EBV; 3) inactivation of intracellular pathways such as HCMV to prevent surface expression of MHC-peptide complexes; or 4) blocking chemokine receptors (e.g., CCR7), resulting in impairment of DC migration to the draining LN (18). These effects on recruitment, maturation, and survival map to our model parameters of Ab-DC frequency, licensing of DCs, and DC life span.

Similarly, data suggest the role of pathogens on inhibition of T cell dynamics. *Bordetella pertussis* generates T regulatory cells that secrete IL-10 and inhibit DC secretion of IL-12, which helps to evade an immune response for whooping cough and suppresses the immune response toward unrelated pathogens (74); this maps in our model to parameters that lead to priming of T cells. Viruses, such as measles or CMV (18, 75, 76), can also interfere with T cell priming, proliferation, and differentiation, probably via blocking or altering cytokine secretion. Each of these types of mechanism is represented in some aspect of our model, and our model suggests that the acquisition of these inhibitory mechanisms by pathogens evolved in the most optimal of ways, because all the tier 1 and tier 2 parameters are used by pathogens to suppress immunity. Although the details of all these mechanisms are not specifically represented in our model structure, they would act to shift the priming and binding curves in Fig. 6 right and/or down. In contrast, if a vaccine or drug were developed to enhance aspects of the DC–T cell interaction, then the curves would move up and/or to the right.

We show here that an *in silico* model can extend knowledge to spatial and temporal scales that fall well outside the range of what is feasible in actual 2PM studies. Specifically, we describe the efficiency of an LN in producing primed CD4+ T cells, demonstrate the influence of particular pathogen-influenced processes on that priming, and we offer insight into the extent to which 2PM studies reflect *in vivo* infections. Our work compliments other computational studies on understanding priming and dynamics of CD8+ T cells (12–14) and the motion of lymphocytes on the fibroblastic reticular cell network within the LN (16, 33). We have now reached the point at which systems biology approaches can simulate the functioning of an entire LN during infection.

Acknowledgments

We acknowledge work done by previous members of our laboratory who helped develop prior versions of model code: Seema Bajaria, Nicholas Perry, Adrienne Walts, and Laura Bickle. We thank Robin Kunkel and Kristen Angonese for artwork, and Joe Waliga for management of material at <http://malthus.micro.med.umich.edu/lab/movies/FULLLN/>. Also, we thank Steve Kunkel and Joanne Flynn for helpful discussions.

Disclosures

The authors have no financial conflicts of interest.

References

- Randolph, G. J., V. Angeli, and M. A. Swartz. 2005. Dendritic-cell trafficking to lymph nodes through lymphatic vessels. *Nat. Rev. Immunol.* 5: 617–628.
- Cahalan, M. D., and I. Parker. 2006. Imaging the choreography of lymphocyte trafficking and the immune response. *Curr. Opin. Immunol.* 18: 476–482.
- von Andrian, U. H., and T. R. Mempel. 2003. Homing and cellular traffic in lymph nodes. *Nat. Rev. Immunol.* 3: 867–878.
- Catron, D. M., A. A. Itano, K. A. Pape, D. L. Mueller, and M. K. Jenkins. 2004. Visualizing the first 50 hr of the primary immune response to a soluble antigen. *Immunity* 21: 341–347.

5. Chiczy, R. M., R. G. Urban, J. C. Gorga, D. A. Vignali, W. S. Lane, and J. L. Strominger. 1993. Specificity and promiscuity among naturally processed peptides bound to HLA-DR alleles. *J. Exp. Med.* 178: 27–47.
6. Miller, M. J., S. H. Wei, I. Parker, and M. D. Cahalan. 2002. Two-photon imaging of lymphocyte motility and antigen response in intact lymph node. *Science* 296: 1869–1873.
7. Miller, M. J., O. Safrina, I. Parker, and M. D. Cahalan. 2004. Imaging the single cell dynamics of CD4+ T cell activation by dendritic cells in lymph nodes. *J. Exp. Med.* 200: 847–856.
8. Miller, M. J., A. S. Hejazi, S. H. Wei, M. D. Cahalan, and I. Parker. 2004. T cell repertoire scanning is promoted by dynamic dendritic cell behavior and random T cell motility in the lymph node. *Proc. Natl. Acad. Sci. U.S.A.* 101: 998–1003.
9. Celli, S., Z. Garcia, H. Beuneu, and P. Bousso. 2008. Decoding the dynamics of T cell-dendritic cell interactions in vivo. *Immunol. Rev.* 221: 182–187.
10. Zheng, H., B. Jin, S. E. Henrickson, A. S. Perelson, U. H. von Andrian, and A. K. Chakraborty. 2008. How antigen quantity and quality determine T-cell decisions in lymphoid tissue. *Mol. Cell. Biol.* 28: 4040–4051.
11. Henrickson, S. E., T. R. Mempel, I. B. Mazo, B. Liu, M. N. Artyomov, H. Zheng, A. Peixoto, M. P. Flynn, B. Senman, T. Junt, et al. 2008. T cell sensing of antigen dose governs interactive behavior with dendritic cells and sets a threshold for T cell activation. *Nat. Immunol.* 9: 282–291.
12. Cella, M., A. Engering, V. Pinet, J. Pieters, and A. Lanzavecchia. 1997. Inflammatory stimuli induce accumulation of MHC class II complexes on dendritic cells. *Nature* 388: 782–787.
13. Rescigno, M., S. Citterio, C. Thèry, M. Rittig, D. Medaglini, G. Pozzi, S. Amigorena, and P. Ricciardi-Castagnoli. 1998. Bacteria-induced neo-biosynthesis, stabilization, and surface expression of functional class I molecules in mouse dendritic cells. *Proc. Natl. Acad. Sci. U.S.A.* 95: 5229–5234.
14. Rudd, B. D., J. D. Brien, M. P. Davenport, and J. Nikolich-Zugich. 2008. Cutting edge: TLR ligands increase TCR triggering by slowing peptide-MHC class I decay rates. *J. Immunol.* 181: 5199–5203.
15. Riggs, T., A. Walts, N. Perry, L. Bickle, J. N. Lynch, A. Myers, J. Flynn, J. J. Linderman, M. J. Miller, and D. E. Kirschner. 2008. A comparison of random vs. chemotaxis-driven contacts of T cells with dendritic cells during repertoire scanning. *J. Theor. Biol.* 250: 732–751.
16. Graw, F., and R. R. Regoes. 2009. Investigating CTL mediated killing with a 3D cellular automaton. *PLOS Comput. Biol.* 5: e1000466.
17. Beltman, J. B., A. F. Marée, J. N. Lynch, M. J. Miller, and R. J. de Boer. 2007. Lymph node topology dictates T cell migration behavior. *J. Exp. Med.* 204: 771–780.
18. Tortorella, D., B. E. Gewurz, M. H. Furman, D. J. Schust, and H. L. Ploegh. 2000. Viral subversion of the immune system. *Annu. Rev. Immunol.* 18: 861–926.
19. McFadden, G., and P. M. Murphy. 2000. Host-related immunomodulators encoded by poxviruses and herpesviruses. *Curr. Opin. Microbiol.* 3: 371–378.
20. Segovia-Juarez, J. L., S. Ganguli, and D. Kirschner. 2004. Identifying control mechanisms of granuloma formation during *M. tuberculosis* infection using an agent-based model. *J. Theor. Biol.* 231: 357–376.
21. Bailey, A. M., B. C. Thorne, and S. M. Peirce. 2007. Multi-cell agent-based simulation of the microvasculature to study the dynamics of circulating inflammatory cell trafficking. *Ann. Biomed. Eng.* 35: 916–936.
22. Thorne, B. C., A. M. Bailey, D. W. DeSimone, and S. M. Peirce. 2007. Agent-based modeling of multicell morphogenic processes during development. *Birth Defects Res. C Embryo Today* 81: 344–353.
23. Thorne, B. C., A. M. Bailey, and S. M. Peirce. 2007. Combining experiments with multi-cell agent-based modeling to study biological tissue patterning. *Brief. Bioinform.* 8: 245–257.
24. Casal, A., C. Sumen, T. E. Reddy, M. S. Alber, and P. P. Lee. 2005. Agent-based modeling of the context dependency in T cell recognition. *J. Theor. Biol.* 236: 376–391.
25. An, G. 2004. In silico experiments of existing and hypothetical cytokine-directed clinical trials using agent-based modeling. *Crit. Care Med.* 32: 2050–2060.
26. Chavali, A. K., E. P. Gianchandani, K. S. Tung, M. B. Lawrence, S. M. Peirce, and J. A. Papin. 2008. Characterizing emergent properties of immunological systems with multi-cellular rule-based computational modeling. *Trends Immunol.* 29: 589–599.
27. Figge, M. T., A. Garin, M. Gunzer, M. Kosco-Vilbois, K. M. Toellner, and M. Meyer-Hermann. 2008. Deriving a germinal center lymphocyte migration model from two-photon data. *J. Exp. Med.* 205: 3019–3029.
28. Mallet, D. G., and L. G. De Pillis. 2006. A cellular automata model of tumor-immune system interactions. *J. Theor. Biol.* 239: 334–350.
29. Beauchemin, C., J. Samuel, and J. Tuszynski. 2005. A simple cellular automaton model for influenza A viral infections. *J. Theor. Biol.* 232: 223–234.
30. Marino, S., S. Pawar, C. L. Fuller, T. A. Reinhart, J. L. Flynn, and D. E. Kirschner. 2004. Dendritic cell trafficking and antigen presentation in the human immune response to *Mycobacterium tuberculosis*. *J. Immunol.* 173: 494–506.
31. Bauer, A., C. Beauchemin, and A. Perelson. 2009. Agent-based modeling of host-pathogen systems: The successes and challenges. *Inf. Sci.* 179: 1379–1389.
32. Marino, S., I. B. Hogue, C. J. Ray, and D. E. Kirschner. 2008. A methodology for performing global uncertainty and sensitivity analysis in systems biology. *J. Theor. Biol.* 254: 178–196.
33. Mueller, S. N., and R. N. Germain. 2009. Stromal cell contributions to the homeostasis and functionality of the immune system. *Nat. Rev. Immunol.* 9: 618–629.
34. Bajénoff, M., N. Glaichenhaus, and R. N. Germain. 2008. Fibroblastic reticular cells guide T lymphocyte entry into and migration within the splenic T cell zone. *J. Immunol.* 181: 3947–3954.
35. Villadangos, J. A., and P. Schnorrer. 2007. Intrinsic and cooperative antigen-presenting functions of dendritic-cell subsets in vivo. *Nat. Rev. Immunol.* 7: 543–555.
36. Carreño, L. J., S. M. Bueno, P. Bull, S. G. Nathenson, and A. M. Kalergis. 2007. The half-life of the T-cell receptor/peptide-major histocompatibility complex interaction can modulate T-cell activation in response to bacterial challenge. *Immunology* 121: 227–237.
37. Lee, B. O., L. Haynes, S. M. Eaton, S. L. Swain, and T. D. Randall. 2002. The biological outcome of CD40 signaling is dependent on the duration of CD40 ligand expression: reciprocal regulation by interleukin (IL)-4 and IL-12. *J. Exp. Med.* 196: 693–704.
38. Spörri, R., and C. Reis e Sousa. 2005. Inflammatory mediators are insufficient for full dendritic cell activation and promote expansion of CD4+ T cell populations lacking helper function. *Nat. Immunol.* 6: 163–170.
39. Blattman, J. N., R. Antia, D. J. Sourdive, X. Wang, S. M. Kaech, K. Murali-Krishna, J. D. Altman, and R. Ahmed. 2002. Estimating the precursor frequency of naive antigen-specific CD8 T cells. *J. Exp. Med.* 195: 657–664.
40. Casroue, A., E. Beaudoin, S. Dalle, C. Pannetier, J. Kanellopoulos, and P. Kourilsky. 2000. Size estimate of the alpha beta TCR repertoire of naive mouse splenocytes. *J. Immunol.* 164: 5782–5787.
41. Mempel, T. R., S. E. Henrickson, and U. H. Von Andrian. 2004. T-cell priming by dendritic cells in lymph nodes occurs in three distinct phases. *Nature* 427: 154–159.
42. Brophy, S. E., L. L. Jones, P. D. Holler, and D. M. Kranz. 2007. Cellular uptake followed by class I MHC presentation of some exogenous peptides contributes to T cell stimulatory capacity. *Mol. Immunol.* 44: 2184–2194.
43. Skokos, D., G. Shakhbar, R. Varma, J. C. Waite, T. O. Cameron, R. L. Lindquist, T. Schwickert, M. C. Nussenzweig, and M. L. Dustin. 2007. Peptide-MHC potency governs dynamic interactions between T cells and dendritic cells in lymph nodes. *Nat. Immunol.* 8: 835–844.
44. Bousso, P., and E. Robey. 2003. Dynamics of CD8+ T cell priming by dendritic cells in intact lymph nodes. *Nat. Immunol.* 4: 579–585.
45. Turner, S. J., P. C. Doherty, J. McCluskey, and J. Rossjohn. 2006. Structural determinants of T-cell receptor bias in immunity. *Nat. Rev. Immunol.* 6: 883–894.
46. Celli, S., F. Lemaître, and P. Bousso. 2007. Real-time manipulation of T cell-dendritic cell interactions in vivo reveals the importance of prolonged contacts for CD4+ T cell activation. *Immunity* 27: 625–634.
47. Obst, R., H. M. van Santen, D. Mathis, and C. Benoist. 2005. Antigen persistence is required throughout the expansion phase of a CD4(+) T cell response. *J. Exp. Med.* 201: 1555–1565.
48. Chang, S. T., J. J. Linderman, and D. E. Kirschner. 2008. Effect of multiple genetic polymorphisms on antigen presentation and susceptibility to *Mycobacterium tuberculosis* infection. *Infect. Immun.* 76: 3221–3232.
49. Utzny, C., D. Coombs, S. Müller, and P. Valitutti. 2006. Analysis of peptide/MHC-induced TCR downregulation: deciphering the triggering kinetics. *Cell Biochem. Biophys.* 46: 101–111.
50. Lee, K. H., A. R. Dinner, C. Tu, G. Campi, S. Raychaudhuri, R. Varma, T. N. Sims, W. R. Burack, H. Wu, J. Wang, et al. 2003. The immunological synapse balances T cell receptor signaling and degradation. *Science* 302: 1218–1222.
51. Smith, C. M., N. S. Wilson, J. Waithman, J. A. Villadangos, F. R. Carbone, W. R. Heath, and G. T. Belz. 2004. Cognate CD4(+) T cell licensing of dendritic cells in CD8(+) T cell immunity. *Nat. Immunol.* 5: 1143–1148.
52. Obregon, C., B. Rothen-Rutishauser, S. K. Gitahi, P. Gehr, and L. P. Nicod. 2006. Exovesicles from human activated dendritic cells fuse with resting dendritic cells, allowing them to present alloantigens. *Am. J. Pathol.* 169: 2127–2136.
53. Théry, C., L. Duban, E. Segura, P. Véron, O. Lantz, and S. Amigorena. 2002. Indirect activation of naïve CD4+ T cells by dendritic cell-derived exosomes. *Nat. Immunol.* 3: 1156–1162.
54. McCune, J. M., M. B. Hanley, D. Cesar, R. Halvorsen, R. Hoh, D. Schmidt, E. Wieder, S. Deeks, S. Siler, R. Neese, and M. Hellerstein. 2000. Factors influencing T-cell turnover in HIV-1-seropositive patients. *J. Clin. Invest.* 105: R1–R8.
55. Sprent, J., and D. F. Tough. 2001. T cell death and memory. *Science* 293: 245–248.
56. Lanzavecchia, A., and F. Sallusto. 2004. Lead and follow: the dance of the dendritic cell and T cell. *Nat. Immunol.* 5: 1201–1202.
57. Lindquist, R. L., G. Shakhbar, D. Dudziak, H. Wardemann, T. Eisenreich, M. L. Dustin, and M. C. Nussenzweig. 2004. Visualizing dendritic cell networks in vivo. *Nat. Immunol.* 5: 1243–1250.
58. Foulds, K. E., L. A. Zenewicz, D. J. Shedlock, J. Jiang, A. E. Troy, and H. Shen. 2002. Cutting edge: CD4 and CD8 T cells are intrinsically different in their proliferative responses. *J. Immunol.* 168: 1528–1532.
59. Bekkhoucha, F., P. Naquet, A. Pierres, S. Marchetto, and M. Pierres. 1984. Efficiency of antigen presentation to T cell clones by (B cell X B cell lymphoma) hybridomas correlates quantitatively with cell surface Ia antigen expression. *Eur. J. Immunol.* 14: 807–814.
60. Demotz, S., H. M. Grey, and A. Sette. 1990. The minimal number of class II MHC-antigen complexes needed for T cell activation. *Science* 249: 1028–1030.
61. Kamath, A. T., S. Henri, F. Battye, D. F. Tough, and K. Shortman. 2002. Developmental kinetics and lifespan of dendritic cells in mouse lymphoid organs. *Blood* 100: 1734–1741.
62. Vermaelen, K. Y., I. Carro-Muino, B. N. Lambrecht, and R. A. Pauwels. 2001. Specific migratory dendritic cells rapidly transport antigen from the airways to the thoracic lymph nodes. *J. Exp. Med.* 193: 51–60.
63. Kirschner, D. E., S. T. Chang, T. W. Riggs, N. Perry, and J. J. Linderman. 2007. Toward a multiscale model of antigen presentation in immunity. *Immunol. Rev.* 216: 93–118.
64. De Boer, R. J., D. Homann, and A. S. Perelson. 2003. Different dynamics of CD4+ and CD8+ T cell responses during and after acute lymphocytic choriomeningitis virus infection. *J. Immunol.* 171: 3928–3935.

65. Celli, S., Z. Garcia, and P. Bousso. 2005. CD4 T cells integrate signals delivered during successive DC encounters in vivo. *J. Exp. Med.* 202: 1271–1278.
66. Takahashi, K., A. Kenji, T. Norihiro, K. Eisaku, O. Takashi, H. Kazuhiko, Y. Tadashi, and A. Tadaatsu. 2001. Morphological interactions of interdigitating dendritic cells with B and T cells in human mesenteric lymph nodes. *Am. J. Pathol.* 159: 131–138.
67. Moon, J. J., H. H. Chu, M. Pepper, S. J. McSorley, S. C. Jameson, R. M. Kedl, and M. K. Jenkins. 2007. Naive CD4(+) T cell frequency varies for different epitopes and predicts repertoire diversity and response magnitude. *Immunity* 27: 203–213.
68. Westermann, J., Z. Puskas, and R. Pabst. 1988. Blood transit and recirculation kinetics of lymphocyte subsets in normal rats. *Scand. J. Immunol.* 28: 203–210.
69. Sant, A. J., F. A. Chaves, S. A. Jenks, K. A. Richards, P. Menges, J. M. Weaver, and C. A. Lazarski. 2005. The relationship between immunodominance, DM editing, and the kinetic stability of MHC class II:peptide complexes. *Immunol. Rev.* 207: 261–278.
70. Lazarski, C. A., F. A. Chaves, S. A. Jenks, S. Wu, K. A. Richards, J. M. Weaver, and A. J. Sant. 2005. The kinetic stability of MHC class II:peptide complexes is a key parameter that dictates immunodominance. *Immunity* 23: 29–40.
71. Yrlid, U., M. Svensson, A. Kirby, and M. J. Wick. 2001. Antigen-presenting cells and anti-*Salmonella* immunity. *Microbes Infect.* 3: 1239–1248.
72. Yrlid, U., and M. J. Wick. 2000. *Salmonella*-induced apoptosis of infected macrophages results in presentation of a bacteria-encoded antigen after uptake by bystander dendritic cells. *J. Exp. Med.* 191: 613–624.
73. Engelmayer, J., M. Larsson, M. Subklewe, A. Chahroudi, W. I. Cox, R. M. Steinman, and N. Bhardwaj. 1999. Vaccinia virus inhibits the maturation of human dendritic cells: a novel mechanism of immune evasion. *J. Immunol.* 163: 6762–6768.
74. McGuirk, P., C. McCann, and K. H. Mills. 2002. Pathogen-specific T regulatory 1 cells induced in the respiratory tract by a bacterial molecule that stimulates interleukin 10 production by dendritic cells: a novel strategy for evasion of protective T helper type 1 responses by *Bordetella pertussis*. *J. Exp. Med.* 195: 221–231.
75. Raftery, M. J., M. Schwab, S. M. Eibert, Y. Samstag, H. Walczak, and G. Schönrich. 2001. Targeting the function of mature dendritic cells by human cytomegalovirus: a multilayered viral defense strategy. *Immunity* 15: 997–1009.
76. Kelleher, P., A. Maroof, and S. C. Knight. 1999. Retrovirally induced switch from production of IL-12 to IL-4 in dendritic cells. *Eur. J. Immunol.* 29: 2309–2318.